Alloying nanoparticles by discharges in liquids: a quest for metastability

Anna V Nominé, Nathalie Tarasenka, Alena Nevar, Mikhail Nedelko, Hiba Kabbara, Alexandre Nomine, Stephanie Bruyere, Jaafar Ghanbaja, Cédric Noël, Andrei Krasilin, et al.

Alloying nanoparticles by discharges in liquids: a quest for metastability

A. V. Nominé[1], N. Tarasenka[2], A. Nevar[2], M. Nedel'ko[2], H. Kabbara[1], A. Nominé[1], S. Bruyère[1], J. Ghanbaja[1], C. Noel[1], A. Krasilin[3,4], G. Zograf[3], V. Milichko[3], N. Kulachenkov[3], S. Makarov[3], N. Tarasenko[2] and T. Belmonte[1]

[1] Université de Lorraine, CNRS, IJL, F-54000 Nancy, France
[2] B.I. Stepanov Institute of Physics, National Academy of Sciences of Belarus
[3] ITMO University, St. Petersburg 197101, Russia
[4] Ioffe Institute, St. Petersburg, Russia

E-mail: thierry.belmonte@univ-lorraine.fr

Received xxxxxx
Accepted for publication xxxxxx
Published xxxxxx

Abstract

Resorting to ultrafast processes to synthesize alloy nanoparticles far from thermodynamic equilibrium is subjected to phase transformations that keep particles at a given temperature for periods of time that are usually long with respect to the process pulse durations. Then, reaching non-equilibrium conditions is not straightforwardly associated with the process, as fast as it can be, but rather to heat transfer mechanisms during phase transformations. This latter aspect is dependent on nanoparticle size. Furthermore, other important phenomena, like chemical ordering, are essential to explain the final structure adopted by an alloy nanoparticle. In this work, a specific attention is paid to suspensions submitted either to electrical discharges or to ultrashort laser excitations. After discussing thermodynamic considerations that give the frame beyond which non-equilibrium alloys form, a description of the heating processes at stake is provided. This leads to maximum temperature reached for particles with nanometric sizes and specific conditions to fulfil practically during the quenching step. The way solidification must be processed in that purpose is discussed next. The example of the Cu-Ag system is finally considered to illustrate the advantage of better controlling processes that are currently used to create homogeneously-alloyed nanoparticles made of immiscible elements, but also to show the actual limitations of these approaches.

Keywords: nanoalloy, metastable state, immiscible elements, electrical discharges, laser processes

1. Introduction

A new challenge in materials science is to increase the performance of nanoparticles up to unprecedented levels for breakthrough achievements in many application fields. For instance, in catalysis, water splitting is still waiting for a extraordinary alloy that would increase the best current yields by, at least, a factor of 2 [1]. In photonics, making possible the activation of strong magnetic modes within the optical range is still an issue [2–4]. Moreover, optical field control at the nanoscale requires mixing semiconductors with high refractive index and plasmonic metals within a single nano-object. It is also a demand in the field of bio- and life-inspired systems [5]. Indeed, the most distinctive design element of living systems is thermodynamic openness. Even though we are still far from creating artificial nanocomponents that could be used to interface chemical fuels and energy-degrading reactions to control their mode of organization, manufacturing

nanoparticles with controlled properties in metastable states is still to master.

Theoretically, the question of the equilibrium state, and thus of the non-equilibrium state, of an alloy particle is complex. It can be understood as the global minimum of the potential energy surface of configurational energy of the given elements arrangement. The solution to the problem of finding the global minimum is most often achieved by global optimization methods. However, intermixing and growth kinetics can suffer from models with unsufficient accuracy to account for the complexity of nanoalloy dynamics. Experimentally, the issue is not more simple. Heating and cooling an alloy nanoparticle considered as an isolated system over a sufficiently large range of temperature and at sufficiently slow rate should necessarily lead to its equilibrium state. However, this condition is not always easy to fulfil but conversely, any change does demonstrate the metastability of the system.

Several seminal works have already shed light on the question of nanoparticles lying in non-equilibrium states. Swiatkowska-Warkocka *et al* [6] claimed that they could grow single-phase uniform AuCo alloy particles with submicrometric sizes (*i.e.* large) and well-defined spherical morphologies by pulsed laser irradiation of Au and Co-oxides nanoparticles dispersed in ethanol. The possibility of alloying immiscible elements into large particles – large being defined later – will be further discussed hereinafter.

Zeng *et al* [7] brought a new concept by considering high concentrations of defects in a structure as a source of metastability. By faulting on purpose nanoscale ZnO through laser ablation in liquid, they measured intense blue emissions for some nanoparticles caused by the presence of defects.

Another method was proposed by Tarasenka *et al* [8]. Improvement of surface and optical characteristics was observed after additional laser post-treatment. Laser induced non-equilibrium liquid chemistry results in surface modification and in enhancement of nanoparticles photoluminescence.

Concerning processes, those based on discharges adopt by far more numerous configurations than those based on laser. There are two main ways to generate a DC discharge in a liquid to synthesise nanoparticles. A low-voltage generator (typically below 1 kV) can be used, which requires to put the two electrodes in contact, the discharge being created when the gap between the electrodes increases, either by material erosion or by mechanical separation. The current [9,10] or the voltage [11] are, most often, used as closed-loop feedback signals to keep the inter-electrode gap distance, measured with a detector, as constant as possible. Resorting to high-voltage discharges (typically beyond 1 kV) enables breakdown at short gaps (i.e. from 100 µm to 1 mm typically, depending to the strength of the dielectric liquid). If one electrode is insulating, AC or RF excitation can also be used.

Experimentally, reactor designs are many, even though it is relatively simple to set up a process as only a power generator, two electrodes and a vessel containing the liquid are required. Indeed, the power source can be used to generate a DC, AC (low frequency), radio frequency, microwave, unipolar pulsed discharge or bipolar pulsed discharge. The electrodes can be a pin, a plate or even materials granules. The shape of the vessel can be a cylinder or a cone to prevent the drift of particles from the discharge zone. The process can be assisted by ultrasound [10,11]. One electrode can vibrate to facilitate electrical breakdown and mix the treated solution [12].

It is also important to mention processes based on other energy sources. We will see that getting alloy nanoparticles from immiscible metals is not process-dependent but mainly ruled by the cooling step, even though each type of process has specificities, mainly during heating steps. For example, it is possible to use microwave sources (see *e.g.* [13, 14]) or plasma sources ([15]). In these two examples, the synthesis of metastable alloy nanoparticles with sizes around 5-10 nm has been claimed by elemental profiles on individual particles. In this paper, we will limit our study to laser processes as a typical case.

In all situations where lasers are used in liquids, the limited number of particles exhibiting the sought-after properties underlines the difficulty of controlling the synthesis process where all steps (alloying, defects control and surface functionalization) are usually merged into a single step. Because of the strong non-equilibrium character of the process, huge gradients affect the homogeneity of the discharge and the composition of the synthesized products.

In this work, the interest of decoupling the different steps described previously is stressed, mainly with the objective of a better control and a better optimization of the whole process. After some thermodynamic considerations, the way particles are heated is described to derive from the maximum temperature reached by nanoparticles conditions for the quenching step. This latter is ruled by solidification processes that are presented next. This paper will be limited to the framework of the treatment of binary suspensions of particles and the example of the Cu-Ag system is selected for illustration.

2. Thermodynamic considerations

Classical nucleation theory stipulates that the formation of nuclei in supersaturated homogeneous solution is governed by the balance between the bulk and surface energies of the new phase.

$$J_{nucl} = A\exp\left(-\frac{E_a}{k_B T}\right)\exp\left(-\frac{\Delta G_{ex}}{k_B T}\right). \qquad (6)$$

The first exponent ($-E_a$ / k_BT) is related to the kinetic barriers with an overall activation energy E_a, while the second exponent ($-\Delta G_{ex}$ / k_BT) represents the thermodynamic barrier.

Parameter *A* is a pre-exponential factor that depends on the properties of the investigated material. It is possible to predict nucleation rates from this equation for any material at a given level of supersaturation. However, as discussed by Gebauer *et al* [16], values calculated accordingly can differ by orders of magnitude from experimental data. Non-classical nucleation theories are needed to fill the gap between predictions of the classical theory and unexplained results.

Resorting to metastable phase diagram (MPD) [17] or size-dependent phase diagram [18] for nanoparticles is sometimes presented as a solution, which is valid when the prevailing conditions are not too far from equilibrium, which means that transitions between phase domains can be predicted by accounting only for the shrinkage of the volume/surface ratio. Otherwise, it is of no use if the expected result is not already known [19] since, basically, nucleation and cluster growth can be dependent upon the existence of multiple local energy minima submitted to local thermal fluctuations.

2.1 Existence of intermediate states

In the non-classical nucleation theory [20], the so-called two-step mechanism assumes that the first step of nucleation is the formation of droplets of dense liquid called clusters (or pre-nucleation clusters – PNCs [21]), due to the critical density fluctuation or phase separation followed by the second step, which is the appearance of crystal nucleus due to structural ordering of atoms or molecules.

In the case of pure metals, when they are free of heterophase impurities, resistance to nucleation is very high [22]. Furthermore, small single-phase nanoparticles are often defect-free [23]. But when it is formed, the solid nucleus grows very fast. In alloys, the interface movement is slower because of rejection of one phase or ordering.

Recent calculations on the solidification of iron melts by molecular dynamics [19] give an overall picture of the first stages of nucleation (**Fig. 1**). Authors showed in this case that the first step of the two-step mechanism could even be divided into 2 parts, leading to 3 sequences:

- first, a fluctuation and competition between crystal-like and icosahedral-like clusters in undercooled melts
- second, the formation and growth of clusters with medium-range order via the transformation of atomic configurations from icosahedral-like to crystal-like
- third, the nucleation of bcc nuclei from the core of steady medium-range order clusters.

This approach sheds light on the difficulty to account for complex molecular interactions prevailing at the very beginning of the process, even for very simple systems made of a single element. The governing kinetics of formation of crystals from clusters possibly adopting intermediate states is a key information to capture, either theoretically or experimentally.

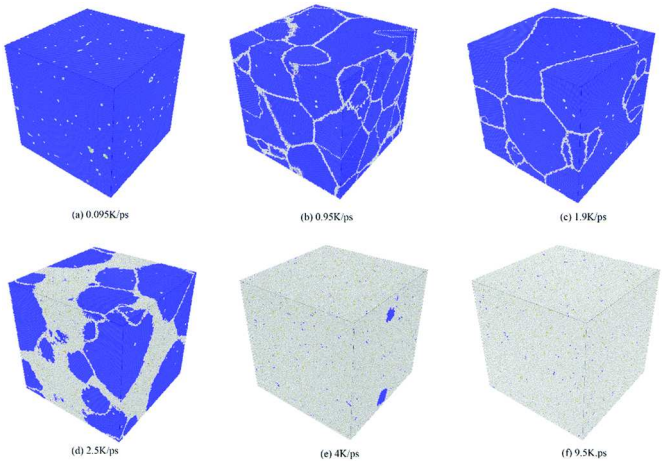

Fig. 1: Snapshots of the simulated solidification structures under different cooling rates of: (a) 0.095 K ps^{-1}, (b) 0.95 K ps^{-1}, (c) 1.9 K ps^{-1}, (d) 2.5 K ps^{-1}, (e) 4 K ps^{-1}, and (f) 9 K ps^{-1}. The blue, red, green, yellow, and grey balls denote bcc, fcc, hcp, ICO, and the other configurations (unknown coordination structures, such as amorphous liquid and solid, grain boundary, and so on), respectively. *Reproduced with permission from the Royal Society of Chemistry, (Fig. 3 p4126 in Ref. [19]).*

2.2 MPD and their input

Let's recall first that a MPD relies on the final states adopted by the mestastable structures according to the experimental conditions.

Binary phase diagrams of immiscible elements are often characterized by an eutectic. The connection of spinodal decomposition to eutectics, in an imposed velocity-dependent temperature gradient, is that a model of eutectics reduces formally to the Cahn-Hilliard model of spinodal decomposition when the fraction of solid becomes sufficiently large, which corresponds to an eutectoid decomposition where the liquid phase would play the role of a glass [24]. Typically, this regime is not expected to be observable in binary alloy eutectics, due to the slow diffusion in solid phase.

However, an eutectic decomposition must not be confused with a spinodal decomposition that takes place everywhere in the system and not only at nucleation sites.

The point is that under rapid cooling, the stable eutectic diagram may transform to embed a new domain referred to as "submerged miscibility gap" [25] or simply as a spinodal domain [26]. From experimental data, this new mestatable phase diagram can be determined (see *e.g.* [27] in the case of the Cu-Ag system). However, the physical phenomena are debated and the role of the surface increase when the particle diameter shrinks on the size of the miscibility gap [28, 29], on thermodynamic parameters like the latent heat [30, 31, 32] or on surface adsorbed states [33] is still debated. As MPDs only

picture the final states, underlying physical phenomena responsible for the transformation are often unclear.

3. Heating nanoparticles

3.1 Differential heating

Let's consider a suspension with two kinds of nanoparticles: one made of one given element (*e.g.* Au or Ag) and one made of another element that is not miscible with the former (*e.g.* Si).

For a given laser fluence ϕ expressed in J m^{-2}, the energy uptake by a given particle is simply:

$$E_{abs} = \sigma_p^{\lambda} \times \phi, \quad (1)$$

where σ_p^{λ} is the absorption cross section in m^2 at the wavelength λ. The values of the absorption cross section can be calculated by describing the interaction between the particle and the electromagnetic plane wave. If the particle is spherical and not too small to neglect quantum effects, then the Mie theory can be used to determine σ_p^{λ}, often by considering an adiabatic assumption. A gold nanoparticle of 50 nm in diameter has the maximum of its absorption cross section close to 540 nm in wavelength whereas a silicon nanoparticle with the same size has its maximum close to 310 nm. The different heating behaviours of each component particle caused by the difference in optical absorption efficiency affects the initial heating step and hence the morphology and inner structure of the products.

To form a non-equilibrium alloy, elements must be mixed. Following Boyer *et al* [34], it is then important to recall that nanoparticles are heated differently according to their thermal properties. The group of M. Sowwan in Okinawa, Japan [35, 36] showed by resorting to a cluster-beams reactor that two essential and successive steps are required. By molecular-dynamics simulations in the silicon–silver binary system, they showed that individual species first form independent clusters of Si and Ag without significant intermixing. Collisions between Si (melt. temp. = 1687 K) and Ag (melt. temp. = 1235 K) are unstable in the early stages of growth (<100 ns) because of large temperature differences that result in rapid energy exchange and separation. Upon further cooling and depletion of isolated Si and Ag atoms through collection by parent clusters (>100 ns), Si–Ag cluster collisions ultimately result in stable hybrid structures.

Consequently, if elements are well separated at the beginning of the process, mixing them requires an incubation time that is different from the heating process by the laser. A sufficiently large number of pulses is then required to move from one step to the other. Of course, the situation is different if elements are already in contact.

It is possible to take advantage of this two-step process to create core-shell structures with uniform shells. In the case of Fe@Au NPs [37], the matching of the gold specific absorption with the wavelength of the laser can be used to fragment Au particles and coat Fe particles with these fragments that are transformed into a compact shell after several pulses. The main drawback of this process is the difficulty to bring to the liquid state both elements simultaneously.

Playing on the initial size distribution could be thought as a way to circumvent this issue. However, nanoparticles undergo fragmentation processes when irradiated by laser, which strongly limits the applicability of the previous idea.

3.2 Fragmentation

Laser-particle interaction processes are clearly separated in time: absorption of photons by electrons (100 fs), heat transfer between the hot electrons and the lattice (<10 ps), melting (30 ps), and heat loss to the surrounding solvent (>100 ps). Then, the use of laser pulses with widths varying over orders of magnitude is by far more efficient for energy deposition with femtosecond lasers than with nanosecond lasers. This has been studied carefully for the photothermal reshaping of gold nanorods in aqueous solution [38]. The energy threshold for complete melting of the nanorods is reduced by two orders of magnitude when using femtosecond lasers. Femtosecond laser pulses have such a high power that the rate of absorption, and thus heating, is extremely fast. A two-temperature model of particle heating under ultrashort pulses has been established by Zhang and Chen [39]. It shows that electrons are overheated during the pulse with respect to the temperature they reach after that, during the equilibrium at the melting point. The particle lattice temperature, on the contrary, is slightly higher than the melting temperature during the pulse (overheating of the solid) but practically constant during the whole melting phase. Consequently, the pulse duration has no strong influence on the melting process. It acts mainly on fragmentation of particles.

Fragmentation can be divided into two regimes depending on the laser intensity. In the first regime, particles are formed by a heating–melting–evaporation mechanism whereby particles are partially vaporized up to a defined laser intensity threshold. In the second regime, they are split by explosion. Then, energy is sufficient to reach an electron deficiency in the particle. A positively charged particle core remains, which undergoes spontaneous fission once the Coulomb forces exceed the cohesive forces in the particle.

This set of unaltered and fragmented particles of one kind has to collide with particles of the other kind in the volume where the laser beam is focused. Furthermore, laser beam absorption must not be affected by the presence of gas bubbles along the beam trajectory. Several strategies have been developed to favour collision between particles and limit interference by bubbles. The use of a stirred by-pass flow cell [40] or a funnel-shaped vessel [41] is a way to improve the collision frequency between particles.

4. Conditions to get homogeneous non-equilibrium alloy

Mixing immiscible elements homogeneously requires the coarsening of liquid droplets and the uniform distribution of the atoms in the mixture. Next, it is necessary to freeze the whole structure with sufficiently strong thermal gradients. Either step requires a specific analysis.

4.1 Coarsening of unalike particles

If unalike particles come to be close or in contact, their coarsening may be driven by various processes.

For small fractions of the minority phase, the Lifshits–Slyozov–Wagner (evaporation–condensation) mechanism is responsible for droplet coarsening: steady diffusion flux from smaller droplets to nearby larger droplets leads to the growth of the latter at the expense of the former. In this mechanism, translational diffusion of component atoms is the main transport process. The average domain size grows proportionally to $(D_0 \times t)^{1/3}$, where t is the time and D_0 the diffusion constant.

For equal fractions of phases, Siggia's mechanism (hydrodynamic coarsening) leads to rapid coarsening. In this mechanism, hydrodynamic flow is the main transport process. The average domain size grows proportionally to $(\sigma / \eta \times t)$, here σ is the interface tension between the two phases and η the viscosity of these phases, which is assumed to be the same for both.

For intermediate cases, coarsening is due to collision between droplets. Shimizu and Tanaka [42] showed that the droplet motion is not brownian, but hydrodynamically driven by the composition Marangoni force due to an interfacial tension gradient produced in each droplet as a consequence of composition correlation among droplets. The average domain size grows proportionally to $t^{1/3}$.

4.2 Freezing all

4.2.1 The role of solidification

When nanoparticles are suspended in the liquid, their cooling is strongly limited by their solidification. It is frequent to read that the conceivable solidification step could happen in the time scale of 10^{-6} to 10^{-5} s, which is much higher than the input pulse duration of the excitation source. For a temperature gradient of 1000 K, this leads to a quenching rate lower than 10^9 K s^{-1}, which is rather low. This means that it should not be possible to produce any metastable alloy by laser treatment of suspension.

The cooling of droplets in suspension is only due to two phenomena: radiation and conducto-convection by the gas phase around the droplet [43]. Radiation cools the droplet and the heat flux (in W) lost by this process is given by:

$$\left.\frac{dq}{dt}\right|_{rad} = \sigma S_p T_p^4 , \qquad (2)$$

$\sigma = 5.67\times10^{-8}$ W m^{-2} K^{-4} is the Stefan-Boltzmann constant, S_p is the particle surface, T_p is the particle temperature. The conducto-convection term is given by:

$$\left.\frac{dq}{dt}\right|_{cc} = hS_p\left(T_p - T_{boil}^{liq}\right), \qquad (3)$$

where h is the heat-transfer coefficient – it does not exceed 5000 W m^{-2} K^{-1} [43] – and T_{boil}^{liq} is the liquid boiling temperature.

It is easy to determine the characteristic times corresponding to each process, which demonstrates that the solidification process of the droplet takes at least 1 µs for most metals considering nanoparticles of about 100 nm in diameter.

It is also easy to show that evaporation is almost nul during solidification because the vapour pressure above the liquid (becoming solid) is extremely weak. In the case of gold:

$$\tau_{evap} \sim 10^6 \times (\tau_{rad} \sim 50 \times \tau_{cc})$$

Some experimental results show clearly that the solidification step controls the final structure of the nanoparticles. The example of the Si-Ag system, characterized by the presence of an eutectic around 1118 K and 89 at.% Ag, is very illustrative. Nomoev *et al* [44] showed that during the crystallisation of the nanoparticle core, eutectics consisting of silver and silicon layers are formed. The cooling rate determines not only the formation of either layered or globular eutectic compounds but also the size of the eutectic plates.

Bharati *et al* [45] synthesized Ag-Cu alloy but what was meant by alloy was an intimate mixing of Cu and Ag phases as shown by the presence of two different inter-planar spacings in a single nanoparticle (0.21 nm for Cu (111) and 0.24 nm Ag (111)). In fact, it is possible to solubilize a weak amount of Cu in Ag (*e.g.* up to 2 at.% at 500 K)and of Ag in Cu (*e.g.* up to 3 at.% at 500 K). Here, the nanoparticle is a mixing of phases (probably small nanoparticles of copper attached to larger silver nanoparticles) and not an alloy. As the solidification process is slow, the particle splits into two almost pure phases.

Several studies considering Au-metal oxide sytems present questionable results. Fuse *et al* [37] produced a mixture of gold and iron oxide. The main argument about the formation of an alloy between the two phases relies on XRD measurements. However, peak shifts and broadening are only interpreted in terms of composition change (Vegard's law), which could be also attributed to the development of strain. This latter mechanism is extremely important in systems where a ductile phase (Au – ~200 Hv) is mixed with a much harder one (Fe_2O_3 – ~1100 Hv). As particles are very large (submicrometric), any substructure showing phase separation cannot be appreciated at this scale. The same reasoning applies also in the two studies by Swiatkowska-Warkocka *et al*. They synthesized Au-Co [6] and Au-Ni [46] submicrometric

particles made of metastable alloys from suspensions of gold with Co_3O_4 and a small fraction of CoO and with NiO. On the contrary, gold-silicon nanoparticles were investigated at high resolution by Larin *et al* [4] who produced phase mixtures by laser ablation of gold thin films deposited on silicon. They showed at low gold contents how the structure of one nanoparticle changes, gold being located at the boundaries between silicon grains that become smaller and smaller when the gold content increases.

As a conclusion, what is often described as "homogeneous" alloys when elements are immiscible, is the coexistence of phases with domain sizes that are small with respect to the particle diameter. Indeed, freezing the structure is not possible directly because of the solidification process.

4.2.2 Solidification dynamics

The dynamics of solidification is extremely complex. It starts with nucleation and the formation of clusters with complex crystallography and it proceeds with cluster growth and the movement of the interface between the two phases. Here, a simplified approach, assuming an already-formed spherical cluster in contact with a liquid phase, is used to evaluate the orders of magnitude of some key parameters of the solidification dynamics. Generally, the movement of the liquid-solid interface is very complex due to the possible development of globular or dendritic structures, associated with microsegregation of impurities by diffusion.

Taken here as a sharp boundary, the interface displacement can be roughly described by using a single formula that gives the interface velocity u_i:

$$u_i \approx \frac{T_m - T_i}{T_i} u_0 \,, \qquad (4)$$

where T_i is the interface temperature [25]. Here, u_0 hides the two main physical phenomena ruling the interface mobility:

- the rearrangement of the growing interface by collision of atoms from the liquid phase with interfacial sites of the solid wall,
- the flux of the crystallization heat at the interface, which is, in the case of droplet in a gas (the liquid phase being vaporized at the droplet temperature), given by the radiative and the conducto-convective terms (Eqs (1) and (2)). This limitation is basically different from the one given in reference [22], where conduction remains.

If, for pure bulk metals, one has $u_0 \sim u_s$, the speed of sound for alloys where diffusive rearrangements may be important, then $u_0 \sim D_l / \lambda$ (where D_l is the diffusion coefficient of species *in the liquid phase* – this point is important hereafter – and λ the interatomic distance). The first situation corresponds to a heat-flow-limited growth whereas the second corresponds to a interface-limited growth, whose magnitude is independent of the way heat is removed.

A heat-flow-limited velocity for a bulk metal is on the order of 2000 m s^{-1}, *i.e.* on the same order of u_s and about 2 orders of magnitude higher than the interface-limited velocity. However, the situation is much different for a liquid droplet surrounded by a gas shell. In this case, $u_0 \sim 1$ cm s^{-1}, *i.e.* 3 orders of magnitude lower than the interface-limited velocity. Consequently, for a nanoparticle, the situation is always limited by the heat flow. Then, Eq. (4) predicts a negligible overheat at the interface.

4.2.3 The maximum size for alloy formation

Conversely, we can estimate from the previous approach the maximum size possible to get an alloyed particle. The case of the Au-Co system is chosen here as an example. The amount of cobalt is supposed to remain low enough not to change significantly the properties of the gold particle but only the crystallization process. Indeed, the presence of an element, even in trace amount, strongly affects the way the alloy crystallizes. The melting temperature varies versus the size of a pure gold particle (typically below 20 nm). There are several approaches that can be used to account for the melting point depression, *i.e.* the decrease in the melting temperature when the particle radius decreases:

- Thermodynamic, known as the homogeneous growth model or HoG, heteregeneous growth model or HeG, liquid shell model (LSM), liquid nucleation and growth (LNG),
- Atomistic, known as Bond-order-length-strength model (BOLS)

These approaches are reviewed in a work by Guenther and Guillon [47]. In the case of gold, it can be described by a reciprocal law if the particle size is larger than 5 nm typically [48]:

$$T_m \text{ [K]} = 1337 - 730 / r_P \text{ [nm]}. \qquad (5)$$

To include sizes below 5 nm, another description is needed and available in [30].

We have to assume that the extracted heat flux is high enough to hinder the separation of phases, which becomes possible when the size of the particle shrinks down to about10 nm or less.

Indeed, Radnóczi *et al*. [23] showed in a remarkable work the role of composition in phase separation of Cu–Ag alloy particles: particles with 15 and 30 at.% Ag contents start separation above 5 nm diameter; in particles of Ag content above 60 at.% Ag this process takes place only above 10 nm diameter. As expected, the particles must be small enough to remove heat sufficiently fast to avoid alloy decomposition. These results are coherent with those published by Malviya *et al* [49] and Yang *et al* [50] in the sense that they demonstrate the need of steeper temperature gradients when the nanoparticle diameter increases. We will see in section 5 that in the case of the Ag-Cu system, the homogeneity of the

smallest nanoalloys is still affected by other segregation processes.

With these data, we can estimate the temperature gradients that are needed to keep immiscible elements in an alloy. Considering an interface velocity of 1 cm s^{-1} for a 5 nm particle, as discussed previously, and a temperature drop from the Cu−Ag eutectic temperature down to room temperature (a variation of ~500 K), one finds a gross estimate of the quenching rate around 10^9 K s^{-1}. Thus, the reason why some works mention the possibility to get alloy of immiscible elements with quenching rates of this order of magnitude is because it is efficient for very small nanoparticles, which however must rely on a relevant elemental characterization.

In these conditions, the regime is no longer heat-limited. So, the process is either controlled by a long nucleation time or by a slow interface. So, superheating is certainly non-negligible here.

Finding a general rule to determine the maximum radius of a particle to keep as an alloy immiscible elements is still a pending question. However, it is possible to consider that it increases by about 1 order of magnitude when the cooling rate increases by 3 orders of magnitude (around 5-10 nm at 10^9 K s^{-1} to 50-100 nm at 10^{12} K^{-1}), which scales with the particle volume.

4.2.4 Speeding up solidification

The quenching process must be fast enough to freeze the atoms in a metastable structure. Vitrification of monoatomic metallic liquids is only possible by achieving liquid-quenching rate of 10^{14} K s^{-1} [51]. At lower rate, metallic glassy structures must include exogenous atoms like boron. This means that the distance crossed by one atom is limited to about one lattice constant $a \sim 5\times10^{-10}$ m for most metals. Taking a self-diffusion coefficient $D_l \sim 5\times10^{-9}$ m^2 s^{-1} corresponding to gold at 1400 K [52], the time needed to diffuse over a is $\tau = (a^2 / 2D_l) = 2.5\times10^{-11}$ s^{-1}. The corresponding temperature gradient that is needed to freeze the structure is then 6×10^{13} K s^{-1}, which is in excellent agreement with the experimental quenching rate given above. This rate determines the front velocity of the solid-liquid interface in the shrinking-core mechanism. This situation corresponds a "heat-flow limited" regime [21].

The diffusion coefficient needed to account for the interface mobility (the jump of an atom from the liquid to the solid phase) is that of the liquid phase. Wang *et al.* [53] identified by molecular dynamics the existence of liquid-like atoms prefiguring in the liquid phase the local disorder appearing close to the solid-liquid interface.

Ultrafast cooling by laser was estimated to lie between typically 10^{12} and 10^{13} K s^{-1} in surface treatment of bulk materials. Of course, these estimates are not valid for particles in suspension where the cooling rate is closer to 10^9 K s^{-1} as mentioned previously. Consequently, in monometallic particles, crystalline phases are always obtained by laser treatment. Nevertheless, cooling rates as high as 10^{12} K s^{-1} are achievable by laser where heat removal is ensured by thermal conduction.

The next question is then to know whether it is possible or not to produce large homogeneously-alloyed nanoparticles from suspensions. Basically, what is needed is an extra source of cooling that can extract heat during the solidification step. This is achievable by putting particles in contact with a mass of matter that plays the role of a heat sink. Two situations arise: make the particle get in contact with a wall or with another cooler (and certainly much bigger) particle.

$$\left.\frac{dq}{dt}\right|_{cond} = k S_p \frac{\partial T_p}{\partial x}, \qquad (7)$$

where k is the thermal conductivity in W m^{-1} K^{-1}. In the first situation, assuming that $\partial T_p / \partial x \approx \left(T_p - T_w\right) / d_p$ where T_w is the wall temperature (taken equal to liquid temperature), one finds with values of k around 1 W m^{-1} K^{-1} corresponding to fused silica or Pyrex which beakers are made of, a characteristic cooling time of about 0.1 ns, leading to a quenching rate of 10^{13} K s^{-1} for gold. This term drastically enhances the heat transfer efficiency of the solidification step by 4 orders of magnitude. Then, it is possible to consider that the formation of metastable particles can be achieved by promoting contacts with walls of bulk materials.

Collision with other alike droplets is assumed to lead to negligible heat transfer, as the collision probability with other particles is assumed to be high when these latter are in the vicinity of the particle under solidification, *i.e.* with similar sizes and temperatures. However, introducing on purpose much larger particles acting as heat sinks, *e.g.* particles with sub-millimetric diameter – ~10^3 times larger than the sought-after nanoparticles – should give a similar result. By stirring the suspension, these heavy beads should have frequent collisions with the nanoparticles and promote heat exchange efficiently.

5. Reassessment of some experimental results: case of the Cu-Ag system

The Cu-Ag system has been studied in detail because of the interest of substituting silver by copper if the use properties are unchanged or even improved. Taner *et al.* [54] and Yang *et al.* [50] showed the higher antibacterial property of small (2 nm in average) Cu-Ag nanoparticles in comparison with other structures. Balkan *et al.* [55] showed that the electrocatalytic performance for oxygen reduction reaction is composition-dependent.

The metastable phase diagram given by Jönsson and Agren [27] was completed by Pandey *et al.* [26] to include the chemical and coherent spinodal boundaries. However, as mentioned before, this description is limited to situations close

to equilibrium. Atanasov *et al.* [56] explain with a Monte Carlo atomistic model that the nanoscale bulk phase diagrams are only relevant to crystalline clusters which are sufficiently large and copper rich. In the general case, the principal interdependence between partial phase compositions and the overall cluster composition in metastable phase diagrams needs to be taken into account. Jabbareh and Monji [57] took into account the effect of the particle size to propose an improved phase diagram.

Malviya *et al*. [49] showed in a remarkable work that phase distribution in small nanoparticles (~20 nm in diameter) is composition-dependent (see **Fig. 2**). Phase segregation is observed at low copper contents. Around 50/50 at.% of each metal, the particle is more homogenous but still exhibits a fine scale segregation. At high silver content, the particle adopts a Cu core–Ag shell structure. Thermodynamics predicts surface segregation of silver that has a lower surface energy than copper (1210 mJ m^{-2} compared to 2130 mJ m^{-2} for Cu). Results by Lu *et al.* [58] are similar.

More generally, two segregation rules apply based on the solid surface energy and atomic size [59]: 1°) if the surface energy of element A is larger than element B, then element B will segregate to the surface ; 2°) when the surface energy difference between two elements is less than ~10% of the highest surface energy, then the element with the largest atomic size segregates to the surface to release the strain energy. This leads easily to "quasi-Janus" arrangements (Fig. 2b).

In **Fig. 2c**, the element profiles are not accurate enough to render the fine scale structure that is clearly visible on the HAADF images. This conclusion points out the impossibility to claim the formation a solid solution simply from elemental profiles if nanoparticles have diameters beyond 20 nm typically. Martinez De La Hoz *et al.* [60] showed that alloying Cu and Ag with more than 1289 atoms at 298 K is not thermodynamically possible, contrary to smaller clusters with 321 and 642 atoms for instance. For nanoparticles with diameters close to 5 nm, homogeneous distributions are measured by TEM, as also shown by Radnóczi *et al*. [23].

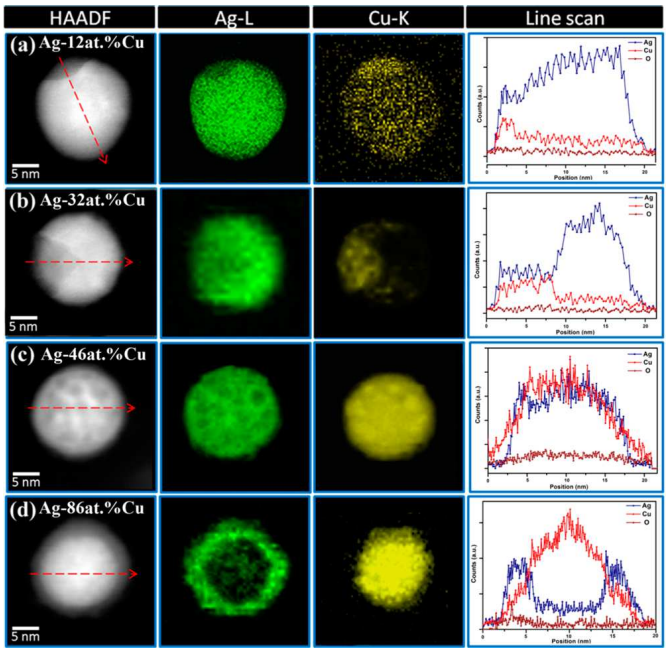

Fig. 2: (a–d) Compositional variation in nanoparticles corresponding to target composition Ag–X atom Cu (X = 20, 40, 60, 80), respectively. The Ag L and Cu K mapping shows the distribution of Ag and Cu elements in the particle. Red arrow on HAADF image shows the position of line scan. An inset in the HAADF image indicates the overall composition of the particle. *Reproduced with permission from ACS Publication, American Chemical Society (Fig. 4 p13232 in Ref. [49]).*

However, the processes are complicated because atomic segregation can be activated by several mechanisms.

According to Núñez and Johnston [61], CuAg clusters with 34, 38, and 98 atoms are subjected to chemical ordering (segregation properties), leading to atomic segregation and Cu core–Ag shell structures. These equilibrium states are not incompatible with homogeneous distributions as those mentioned previously since the latter are supposed to be far from equilibrium.

Langlois *et al.* [62] understood that the competition existing between the growth and the ordering kinetics governs the nanoparticle structure but, in contrast with Malviya's work, they did not consider the effect of composition over a sufficiently large range. Using a co-evaporation process where the cooling rate of nanoalloys is rather slow, they noticed the formation of phase segregation in particles with sizes beyond 12 nm and core/shell structures below this threshold. They showed that the growth of the Ag shell is more isotropic for diameters below 10 nm, which leads to a more homogeneous shell around the Cu core. The core-shell structure would be favoured by the presence of (111) facets at the surface of the Cu core structure, which is either icosahedral or decahedral if the particle size is smaller than 8 nm. Then, the Cu core never

adopts the third possible structure found on pure Cu particles: a rounded or faceted monocrystalline fcc structure.

Asagari *et al*. [63] determined the kinetic rates of atomistic inter-diffusion mechanisms leading to putative global minima in metastable configurations exhibiting single-atom misplacements due, *e.g.*, to imperfect synthesis. These rates vary with the adopted reordering behaviour by 10–11 orders of magnitude in rates at room temperature in narrow intervals of size and composition. Thus, equilibration of $Ag_{29}Cu_5$ occurs in tens of nanoseconds but it takes minutes for $Ag_{25}Cu_7$. Rearrangements occur via collective and strongly cooperative moves related to Ag surface diffusion, in agreement with thermodynamics.

Therefore, the atomic structure of clusters strongly affects segregation. A number of stable structures made of a small number of atoms, with magic numbers, was determined by modelling.

In general, the trend is the following one [64, 65]. For a given size, compact polyicosahedral structures have a large number of nearest-neighbour bonds (NN-bonds) that are strained because inner bonds are compressed, while surface bonds are expanded. In pure metals, surface bonds must be shorter than inner bonds because of a favourable bond order–bond length correlation. If the inner atoms in a pure cluster are substituted by atoms of smaller size, the strain is relieved. The Ag-Cu system is characterized by considerable size mismatch, and by the tendency of silver atoms that are larger (172 vs 140 pm) to segregate to the surface. Therefore, core-shell polyicosahedra are the lowest-energy structures for Ag-rich compositions, and perfect core-shell arrangements correspond to enhanced stability. However, polyicosahedral structures are present for a wide range of compositions, extending to the Cu-rich side in Ag-Cu. This shows that the presence of two different elements helps in any case to relieve the strain, thus favouring structures with a large number of nearest-neighbour bonds [66].

Magic sized clusters of Cu_mAg_n nanoalloys with $m+n$ ranging from 2 to 60 were determined by Molayem *et al.* [66]. Momim and Bhowmick [67] studied the formation of free bimetallic clusters between Cu and Ag up to 7100 a.m.u. The results produce evidence of magic combination: 1465 binary Cu_mAg_n nanoclusters are identified in which many magic compositions appear with higher abundances. Overall, it is observed that Cu and Ag atoms do not mix randomly but preferably surface segregate.

Quantum effects can also contribute to stabilize magic configurations, but this can be detrimental to rearrangement kinetics if the system gets trapped into configurations sharing magic features with the global minimum, but not with the intermediate configurations connecting them.

Bochicchio *et al.* [68] studied segregation patterns of Ag–Cu nanoparticles adsorbed on MgO (001). The role of the presence of an oxide surface on segregation was found to be meaningful: on increasing the Ag content, the structure of the cluster deposited on MgO, which is often a kind of half core-shell type, follows a sequence: faulted fcc → icosahedral → fcc. Some Cu atoms are always found at the interface with the substrate even for quite Ag-rich compositions, due to the high interaction of copper with MgO.

The control of chirality can dramatically enhance the optical activity of metallic nanoparticles [69]. Chirality in nanostructures results either from chiral shapes, from chiral assemblies or from the ligands grafted onto nanoclusters [70]. In the last case, chirality results either from the intrinsic chirality of the metal core, from the core-ligand interface or from the chiral arrangement of the ligands [71, 72]. In the case AgCu nanoalloys, the chirality in these structures is either due to the rearrangement of the Ag shell with achiral Cu core (and particles are spherical) [73] or to a chiral Cu core – Ag shell (and particles are non-spherical – **Fig. 3**) [74].

These chiral nanoalloys have similar stability as the Ag-rich nanoalloys like "magic" sized icosahedra mentioned earlier. However at a fixed size, they also have very high stability in terms of chemical composition.

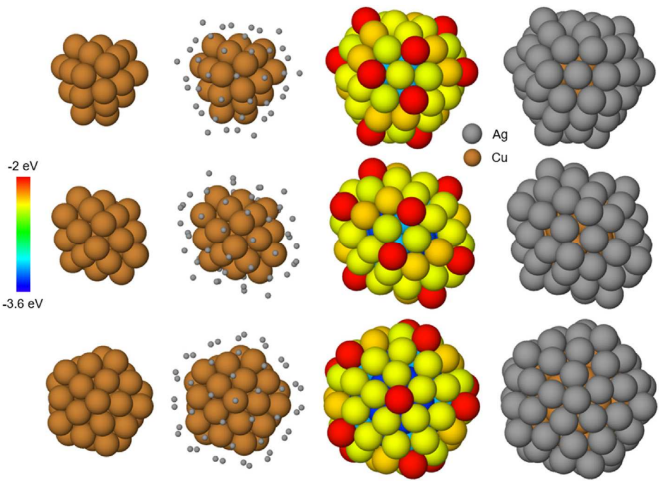

Fig. 3: Arrangement of the Ag shells (columns 2 to 4) in the lowest sized nanoalloys $Ag_{52}Cu_{28}$ (first row, T symmetry), $Ag_{56}Cu_{32}$ (second row, D3 symmetry), and $Ag_{62}Cu_{39}$ (third row, C5 symmetry). The chiral Cu core in each of the nanoalloys is shown in the first column. The color coding in the third column refers to the energy of the atoms. *Reproduced with permission from Elsevier, (Fig. 2 p4 in Ref. [74]).*

Another key step to consider after or even during synthesis is the oxidation step that strongly affects chemical ordering. This has been shown clearly by Pellarin *et al.* [75]. Air oxidation of Cu core-Ag shell structures induces an outward segregation of copper in nanoparticles of about 5 nm in diameter, leading to the formation of a Cu_2O oxide shell. Indeed, copper affinity toward oxygen is higher than silver. Such a change in the nanoparticle structure leads to a localized

surface plasmon resonance peak that is all the more shifted toward low energy as the oxide thickness is large.

Recently, the same idea was applied to selective dealloying [76]. By selective leaching the exposed less noble metals (*e.g.*, Co, Ni, and Cu) under potential control, the dealloyed catalysts form an incompletely noble metal shell (about three to five atomic layers deep) exposing more plentiful stepped surface and active site [77] that significantly improve the activity and stability of the alloy.

Yang *et al.* [50] showed examples of "homogeneously alloyed" nanoparticles. The lack of resolution is probably responsible for the apparent homogeneity of the particle composition and structure. It seems improbable as results were obtained in conditions where the quenching rate was too slow to freeze a final state in a liquid-like configuration. The essential point here is to understand that the homogeneity must be characterized at a scale that is equal to or lower than the scale at which segregation is driven by thermodynamics. For instance, Li and Chen [78] showed that the Ag_6Cu_7 cluster is a Janus-separated cluster, *i.e.* non-homogenous, but the Ag_7Cu_6 cluster is amorphous and does show an Ag–Cu alloyed motif. This confirms the need for an ultrafast cooling rate and a characterization at the atomic level for tiny clusters.

6. Conclusion

Getting homogeneously-alloyed nanoparticles made of immiscible elements requires ultra-high quenching rates. As heat removal is strongly limited if nanoparticles are in a gas or in a liquid, contact with highly conductive solid surfaces is mandatory to create nanoalloys. Atoms in the liquid phase during the quenching step must only have a very limited distance over which they can diffuse to avoid segregation.

The cooling process of a spherical nanoparticle follows a shrinking-core model. In large particles, typically beyond 20 nm, heat removal takes longer as it is also limited by the size of the object. Then, the atomic diffusion length is longer in the core than in the shell of the particle.

For small nanoparticles, typically below 10 nm, segregation of elements is subjected to various mechanisms depending on the particle composition, size via quantum effects, defects, surface functional groups, oxidation, contact with a substrate... Then, it is very difficult to get homogeneous alloy too.

Properties resulting from the nanoparticle structure and composition can change dramatically. They are also dependent on defects. Correlations are yet not so straightforward to establish. Indeed, characterization of nanoparticles can be misleading if information is not collected with a sufficiently high resolution. Once this milestone reached, mastering the design of nanoparticles opens up the way to materials with higher efficiency for many applications.

Acknowledgments

The authors acknowledge the French PIA (programme d'investissements d'avenir) project Lorraine Université d'Excellence (Ref. ANR-15-IDEX-04-LUE) for financial support.

ORCID iDs

N Tarasenka https://orcid.org/0000-0001-7902-7932
A Nominé https://orcid.org/0000-0002-5553-3539
A. Nevar https://orcid.org/0000-0001-9535-0385
M. Nedel'ko https://orcid.org/0000-0001-7183-7367
H. Kabbara https://orcid.org/0000-0003-4082-7136
A V Nominé
S. Bruyère https://orcid.org/0000-0001-7160-4520
J. Ghanbaja https://orcid.org/0000-0003-2870-0570
C. Noel https://orcid.org/0000-0001-8651-1423
A. Krasilin https://orcid.org/0000-0002-3938-3024
G. Zograf https://orcid.org/0000-0003-0791-5636
V Milichko https://orcid.org/0000-0002-8461-0804
N. Kulachenkov https://orcid.org/0000-0001-9460-8727
S. Makarov https://orcid.org/0000-0002-9257-6183
N. Tarasenko https://orcid.org/0000-0002-2222-9389
T Belmonte https://orcid.org/0000-0002-8572-7676

References

[1] Wang Q and Domen K 2020 *Chem. Rev.* **120** 919
[2] Krasnok A, Makarov S, Petrov M, Savelev S, Belov P and Kivshar Y 2015 *Proc. SPIE* **9502** 950203
[3] Kuznetsov A I, Miroshnichenko A E, Brongersma M L, Kivshar Y S and Luk'yanchuk B 2016 *Science* **354** aag2472
[4] Larin A O *et al* 2020 *Nanoscale* **12** 1013
[5] Grzybowski B A and Huck W T S 2016 *Nature Nanotechnol.* **11** 585
[6] Swiatkowska-Warkocka Z, Koga K, Kawaguchi K, Wang H, Pyatenko A and Koshizaki N 2013 *RSC Advances* **3** 79
[7] Zeng H, Duan G, Li Y, Yang S, Xu X, and Cai W 2010 *Adv. Funct. Mater.* **20** 561
[8] Tarasenka N, Stupak A, Chakrabarti S, Mariotti D, and Tarasenko N 2017 *ChemPhysChem.* **18** 1074
[9] Karahaliou P K, Svarnas P, Georga S N, Xanthopoulos N I, Delaportas D, Krontiras C A, and Alexandrou I 2012 *J. Nanopart. Res.* **14** 1297
[10] Bera D, Brinley E, Kuiry S C, McCutchen M, Seal S, Heinrich H, and Kabes B 2005 *Rev. Sci. Inst.* **76** 033903
[11] Horváth Z E, Kertész K, Pethő L, Koós A A, Tapasztó L, Vértesy Z, Osváth Z, Darabont Al, Nemes-Incze P, Sárközi Zs, and Biró L P 2006 *Curr. Appl. Phys.* **6** 135
[12] Mizukoshi Y, Hori F, and Okitsu K 2017 *Jap. J. Appl. Phys.* **57** 0102A5

[13] Guo H *et al* 2018 *ACS Catal.* **8** 11386
[14] García S, Zhang L, Piburn G W, Henkelman G and Humphrey S M 2014 *ACS Nano* **8** 11512
[15] Panuthai N, Savanglaa R, Praserthdam P and Kheawhomn S 2014 *Jpn. J. Appl. Phys.* **53** 05HA11
[16] Gebauer D, Kellermeier M, Gale J D, Bergströmc L and Cölfen H 2014 *Chem. Soc. Rev.* **43** 2348
[17] Shu Y, Ando T, Yin Q, Zhou G and Gu Z 2017 Nanoscale **9** 12398
[18] Zhang L, Yu G, He X, Li S, Ning W and Wang X 2019 J. Alloy. Comp. **772** 209
[19] Zhang Q, Wang J, Tang S, Wang Y, Li J, Zhou W and Wang Z 2019 *Phys. Chem. Chem. Phys.* **21** 4122
[20] Karthika S, Radhakrishnan T K and Kalaichelvi P 2016 *Cryst. Growth Des.* **16** 6663
[21] Lin C-J, Spaepen F and Turnbull D 1984 J. *Non-Cryst. Solids* 61 & 62 (1984) 767
[22] Poate J M and Mayer J W 1982 *Laser annealing of semiconductors* Edited by Academic Press Inc., Spaepen F and Turnbull D, Chap. **2** 15
[23] Radnóczi G, Bokányi E, Erdélyi Z and Misják F 2017 *Acta Materialia* **123** 82
[24] Drolet F, Elder K R, Grant M and Kosterlitz J M 2000 *Phys. Rev. E* **61** 6705
[25] Liu D, Jie J, Dong B, Guo Z, Wang T and Li T 2018 *Mater. Design* **156** 71
[26] O.P. Pandey, S.N. Ojha and S. Lele 1993 *Script. Metall. Mater.* **29** 1131
[27] Jönsson B and Agren J 1988 *J. Less Common Metals* **145** 153
[28] Burch D and Bazant M Z 2009 *Nanoletters* **39** 3795
[29] Tang M, Huang H-Y, Meethong N, Kao Y-H, Craig Carter W and Chiang Y-M 2008 *MRS Symposium Proceedings* **1100** JJ03-04
[30] Font F, Myers T G 2013 *J. Nanopart. Res.* **15** 2086
[31] Ercolessi F, Andreoni W and Tosatti E 1991 *Phys. Rev. Lett.* **66** 911
[32] Sheng HW, Ren G, Peng LM, Hu ZQ and Lu K 1996 *Phil. Mag. Lett.* **73** 179
[33] Zaghib K, Mauger A, Gendron F and Julien C M 2008 *Chem. Mater.* **20** 462
[34] Boyer P, Menard D and Meunier M 2010 *J. Phys. Chem. C* **114** 13497
[35] Mattei J-G, Grammatikopoulos P, Zhao J, Singh V, Vernieres J, Steinhauer S, Porkovich A, Danielson E, Nordlund K, Djurabekova F and Sowwan M 2019 *Chem. Mater* **31** 2151
[36] Singh V, Cassidy C, Grammatikopoulos P, Djurabekova F, Nordlund K and Sowwan M 2014 *J. Phys. Chem. C* **118** 13869
[37] Fuse H, Koshizaki N , Ishikawa Y and Swiatkowska-Warkocka Z 2019 *Nanomater.* **9** 198
[38] S. Link, C. Burda, B. Nikoobakht, and M. A. El-Sayed 2000 *J. Phys. Chem. B* **104** 6152
[39] Zhang Y, Chen J K 2008 J. *Appl. Phys.* **104** 054910
[40] Semaltianos N G 2010 *Crit. Rev. Solid State Mater. Sci.* **35** 105
[41] Mardanian M, Nevar A A, Nedel'ko M and Tarasenko N V (2013) *Eur. Phys. J. D* **67** 208
[42] Shimizu R and Tanaka H 2015 *Nature Communication* **6** 7407
[43] Pyatenko A, Wang H, Koshizaki N and Tsuji T 2013 *Laser Photonics Rev.* **7** 596
[44] Nomoev A V, Torhov N A, Khartaeva E Ch, Syzrantsev V V, Yumozhapova N V, Tsyrenova M A and Mankhirov V N 2019 *Chem. Phys. Lett.* **720** 113
[45] Bharati M S S, Chandu B and Venugopal Rao S 2019 *RSC Adv.***9** 1517
[46] Swiatkowska-Warkocka Z, Pyatenko A, Krok F, Jany B R and Marszalek M 2015 *Sci. Rep.* **5** 09849
[47] Guenther G and Guillon O 2014 *J. Mater. Sci.* **49** 7915
[48] Vollath D, Fischer F D and Holec D 2018 Beilstein J. Nanotechnol. **9** 2265
[49] Malviya K D and Chattopadhyay K 2014 *J. Phys. Chem. C* **118** 13228
[50] Yang L *et al.* 2019 Colloids Surf. B: Biointerf. **180** 466
[51] Zhong L, Wang J, Sheng H, Zhang Z and Mao S X (2014) *Nature* **512** 177
[52] Akhter J I, Ahmed E, Ahmad M 2005 *Mater. Chem. Phys.* **93** 504
[53] Wang N, Rokhlin S I and Farson D F 2008 *Nanotechnol.* **19** 415701
[54] Taner M, Sayar N, Yulugband I G and Suzer S 2011 *J. Mater. Chem.* **21** 13150
[55] Balkan T, Küçükkeçeci H, Zarenezhad H, Kaya S and Metin Ö 2020 *J. Alloys Comp.* **831** 154787.
[56] Atanasov I, Ferrando R and Johnston R L 2014 *J. Phys.: Condens. Matter* **26** 275301
[57] Jabbareh M A and Monji F 2018 *Calphad* **60** 208
[58] Lu P, Chandross M, Boyle T J, Clark B G and Vianco P 2014 *Appl. Phys. Lett. Mater.* **2**, 022107
[59] Cui M, Lu H, Jiang H, Cao Z and Meng X 2017 *Sci. Reports* **7** 41990
[60] Martinez De La Hoz J M, Callejas Tovar R and Balbuena P B 2009 *Molec. Simul.* **35** 785
[61] Núñez S and Johnston R L 2010 *J. Phys. Chem. C* **114** 13255
[62] Langlois C, Alloyeau D, Le Bouar Y, Loiseau A, Oikawa T, Mottet C and Ricolleau C 2008 *Faraday Discuss.* **138** 375
[63] Asgari M, Negreiros F R, Sementa L, Barcaro G, Behnejad H and Fortunelli A 2014 *J. Chem. Phys.* **141** 041108
[64] Rossi G, Rapallo A, Mottet C, Fortunelli A, Baletto F and Ferrando R 2004 *Phys. Rev. Lett.* **93** 105503
[65] Rapallo A, Rossi G, Ferrando R, Fortunelli A, Curley B C, Lloyd L D, Tarbuck G M and Johnston R L 2005 *J. Chem. Phys.* **122** 194308
[66] Molayem M, Grigoryan V G and Springborg M 2011 *J. Phys. Chem. C* **115** 22148
[67] Momim T and Bhowmick A 2013 *J. Alloys Comp.* **559** 24
[68] Bochicchio D, Ferrando R, Panizon E and Rossi G 2016 *J. Phys.: Condens. Matter* **28** 064005
[69] Schaaff T G and Whetten R L 2000 *J. Phys. Chem. B* **104** 2630
[70] Pelayo J J, Valencia I, García A P, López M, Toffoli D, Stener M, Fortunelli A and Garzón I L 2018 *Adv. Phys. X* **3** 965
[71] Noguez C and Garzón I L 2009 *Chem. Soc. Rev.* **38** 757
[72] Zeng C and Jin R 2017 *Chem. Asian J.* **12** 1839
[73] Bochicchio D and Ferrando R 2010 Nano Lett. **10** 4211
[74] Settem M 2020 *J. Alloys Comp.* **844** 155816

[75] Pellarin M, Issa I, Langlois C, Lebeault M A, Ramade J, Lermé J, Broyer M and Cottancin E 2015 *J. Phys. Chem. C* **119** 5002
[76] Wu X, Chen F, Zhang N, Qaseem A and Johnston R L 2017 *small* **13** 1603876
[77] Mani P, Srivastava R and Strasser P 2008 *J. Phys. Chem. C* **112** 2770
[78] Li W and Chen F 2013 *J. Nanopart. Res.* **15** 1